Behavior of liquid hydrogen inside an ICF target[1]

K. Kim and L. Mok

Department of Electrical Engineering, University of Illinois
Urbana, Illinois 61801

T. Bernat

Lawrence Livermore National Laboratory
Livermore, California 94550

Abstract

The configuration of liquid hydrogen inside a spherical glass shell ICF target has been studied both theoretically and experimentally. Because of the zero contact angle between the D_2 liquid and glass substrate and the limited wetting surface that is continuous, the liquid hydrogen completely covers the interior of the glass shell, resulting in the formation of a void at the center. For this reason, the present problem distinguishes itself from that for a sessile drop sitting on a flat surface. A theory has been formulated to calculate the liquid hydrogen configuration by including the London-dispersion force between the liquid and the substrate molecules. The net result is an augmented Bashforth-Adams equation appropriate to a spherical substrate, which is considered to be the major contribution of the present work. Preliminary calculations indicate that this new equation accurately models the liquid hydrogen behavior inside a spherical microshell.

Introduction

In the inertial confinement fusion (ICF) research, one of the important tasks is to find an optimum target design which can achieve sufficiently high fuel density with minimum compression energy input. Various target designs have been proposed.[2-4] Among them is a cryogenic target, which consists of a hollow uniform shell of liquid or solid DT (Deuterium-Tritium mixture) condensed onto the inner surface of a glass microballoon (GMB). Mason[4] has theoretically predicted that such targets will give higher fusion yields. Recently, from the preliminary results of their target implosion experiment, Henderson and his coworkers[5] have noted that neutron yields are enhanced by a factor of ten or more when a cryogenic DT target is used instead of a gas DT target.

Because of this preliminary finding (which needs further investigation), the cryogenic targets are currently attracting a fair amount of attention. Several techniques have been developed to fabricate these targets.[5-13] However, difficulties have been encountered, especially in conjunction with producing and maintaining a uniform liquid layer inside the GMB. Some researchers have obtained a liquid spheroid on one side of the GMB, whereas others have produced a continuous liquid layer, more often with one side thinner than the other.

Shown in Figure 1 are the micrographs of a D_2-filled GMB target, 320 μm in diameter, 15 μm in thickness, and filled with approximately 700 atm of D_2 gas at room temperature. Figures 1a and 1b are, respectively, the shadow and interference micrographs of the target at room temperature. The corresponding pictures taken at a temperature (~25 K) below the liquefaction point of D_2 are shown in Figures 1c and 1d. The interference micrographs were obtained using a home-made Mach-Zehnder interference microscope.

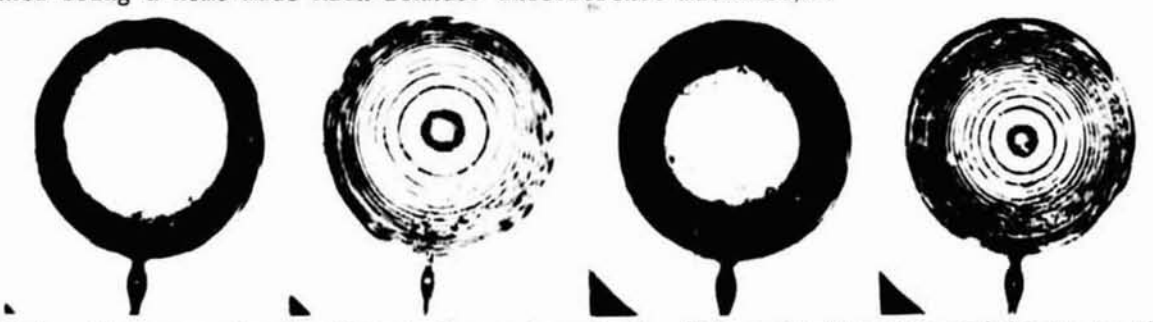

Figure 1. Pictures of a D_2-filled glass microshell, 320 μm in diameter and 15 μm in thickness, filled with approximately 700 atm of D_2 gas at room temperature. Figure 1a. Shadow micrograph at room temperature; Figure 1b. Interference micrograph at room temperature; Figure 1c. Shadow micrograph of the target with a continuous liquid-D_2 layer at a cryogenic temperature; Figure 1d. Interference micrograph of the same target in Figure 1c.

One distinct feature exhibited by Figure 1 is that the liquid D_2 formed inside the GMB spreads out and completely wets the entire substrate. The net result is a continuous liquid layer having a gas void inside of it. This situation is particularly interesting, not only because it is unique (note that one cannot achieve the same situation with a sessile drop sitting on a flat surface), but also because it offers a promising possibility for fabricating a uniform layer of DT-condensate inside an ICF target.

Presented in this paper is an in-depth study of the behavior of a liquid inside a spherical microshell (SMS). First, a physical model is formulated to predict the liquid profile inside the SMS. These theoretical predictions are then compared with the experimental results obtained for a GMB containing liquid hydrogen. It is hoped that this study will result in a reliable scheme for producing and maintaining a uniform layer of DT-condensate inside a cryogenic ICF target.

Theories for the profile of liquid inside a spherical microshell

For the convenience of presentation, we first formulate a simple theory applicable to a liquid contained in a spherical substrate. Then, after showing that the theory is incapable of describing a continuous liquid layer wetting the entire substrate - namely, that it is only appropriate to a liquid layer having a well-defined line of contact between the substrate, liquid, and vapor, it is extended by including the van der Waals attraction between the liquid and the substrate molecules. This latter theory, as will be shown, does have the properties appropriate for describing a continuous liquid layer and, therefore, constitutes a major contribution of the current work.

Profile of liquid with contact line inside a spherical microshell

Following Gibbs[14], we calculate the minimum energy configuration of the liquid enclosed in an SMS using the calculus of variations. Consider a coordinate system shown in Figure 2a where the thick solid line represents the inner surface of the GMB. For the moment, we consider the gravitational force and the interfacial tensions at the liquid-vapor, liquid-solid and solid-vapor interfaces as the major forces contributing to the energy of the system. Providing that the profile of the liquid-vapor interface is symmetric about the $\tilde{y}$-axis, the total energy of the system can, therefore, be expressed as the sum of the following terms.

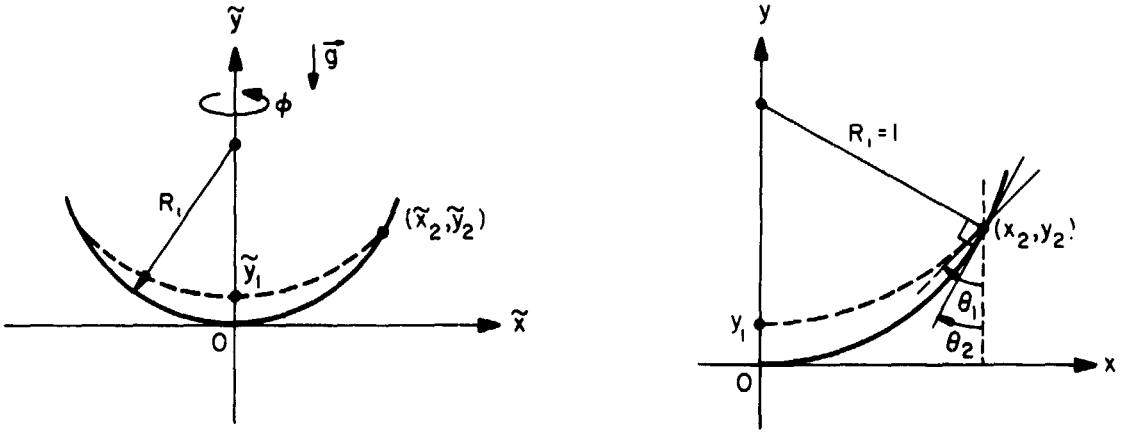

Figure 2. (a) Cylindrical coordinate system employed for the description of a spherical target. (b) The cylindrical system shown above redefined in dimensionless units.

$$E_g = \rho g \int_{V_L} \tilde{y}\, dv = 2\pi \int_{\tilde{y}_1}^{\tilde{y}_2} \tfrac{1}{2} \rho g\, \tilde{y}[R_i^2 - (\tilde{y} - P_i)^2 - \tilde{x}^2]\, d\tilde{y} \tag{1}$$

$$E_{LV} = \gamma_{LV} \int_{S_{LV}} ds = 2\pi \int_{\tilde{y}_1}^{\tilde{y}_2} \gamma_{LV}\, \tilde{x}[1 + (\tilde{x}')^2]^{\frac{1}{2}}\, d\tilde{y} \tag{2}$$

$$E_{SL} = \gamma_{SL} \int_{S_{SL}} ds = 2\pi \int_{\tilde{y}_1}^{\tilde{y}_2} \gamma_{SL} R_i \, d\tilde{y} \tag{3}$$

$$E_{SV} = \gamma_{SV} \int_{S_{SV}} ds = \text{Constant} - 2\pi \int_{\tilde{y}_1}^{\tilde{y}_2} \gamma_{SV} R_i \, d\tilde{y} \tag{4}$$

where ρ is the density of liquid; g is the gravitational acceleration; V_L is the volume of the liquid, γ_{LV}, γ_{SL}, and γ_{SV} are the interfacial tensions at the liquid-vapor, solid-liquid and solid-vapor interfaces (S_{LV}, S_{SL}, and S_{SV}), respectively; R_i is the inner radius of the SMS; and $\dot{x} = d\tilde{x}/d\tilde{y}$.

The variations are now subject to the constraint of the enclosed liquid volume, which is constant for a given temperature and gas fill pressure (e.g., N_2 pressure) of the SMS. (Note that the thermal energy of the system, which is also a constant at a given temperature, is uniquely determined once the liquid volume is specified, and, therefore, not specifically considered.) The expression of the liquid volume in this case is

$$V_L = \text{Constant} + 2\pi \int_{\tilde{y}_1}^{\tilde{y}_2} \tfrac{1}{2}[R_i^2 - (\tilde{y} - R_i)^2 - \tilde{x}^2] \, d\tilde{y} \tag{5}$$

Combining Eqs. (1) through (5), and carrying out the mathematics required to arrive at the Euler equation[15], one obtains

$$\frac{\tilde{x}''}{[1 + (x')^2]^{3/2}} - \frac{1}{\tilde{x}[1 + (\tilde{x}')^2]^{\frac{1}{2}}} = -\frac{\rho g \tilde{y} + \lambda}{\gamma_{LV}} , \tag{6}$$

where $\tilde{x}'$ and $\tilde{x}''$, respectively, denote the first and second derivatives of $\tilde{x}$ with respect to $\tilde{y}$, and λ is the usual Lagrange multiplier resulting from the constraint of constant liquid volume. The absence of the solid-liquid and solid-vapor interfacial tensions, γ_{SL} and γ_{SV}, in Eq. (6) was to be expected since the corresponding interfacial energy terms, E_{SL} and E_{SV}, depend only on the two end points $\tilde{y}_1$ and $\tilde{y}_2$, which remain unchanged during the process of calculus of variations.

Letting

$$x = \frac{\tilde{x}}{R_i} \quad , \quad y = \frac{\tilde{y}}{R_i} \quad , \quad \alpha = \frac{\lambda R_i}{\gamma_{LV}} \text{ and } \beta = \frac{\rho g R_i^2}{\gamma_{LV}} \quad , \tag{7}$$

the dimensionless form of Eq. (6) is obtained as

$$\frac{x''}{[1 + (x')^2]^{3/2}} - \frac{1}{x[1 + (x')^2]^{\frac{1}{2}}} = -(\alpha + \beta y) \tag{8}$$

Two end-point conditions are needed to close this equation. They are

1. $x' = \infty$ at $x = 0$ (9a)

2. $x(y) = [1 - (y - 1)^2]^{\frac{1}{2}}$ at $y = y_2$ (9b)

The first condition simply states that the liquid profile is symmetric about the $\tilde{y}$-axis. The second condition is the so-called transversality condition[15] - that is, at $y = y_2$ the liquid-vapor interface lies on the inner surface of the SMS. It is easy to verify that the second condition gives rise to Young's equation[16] for the contact angle, θ, i.e.,

$$\cos \theta = \cos (\theta_1 - \theta_2) = \frac{\gamma_{SV} - \gamma_{LS}}{\gamma_{LV}} \tag{10}$$

The definitions of the angles θ_1 and θ_2 are given in Fig. 2b.

Note that Eq. (6) is reduced to the equation derived earlier by Bashforth and Adams for a sessile drop[17] if the origin of the coordinate system is shifted to $x = 0$ and $y = y_1$, and the normalization variable is replaced by the radius of curvature at the origin. So, we henceforth, refer to Eq. (6) (or Eq. (8)) as the Bashforth - Adams equation. The original derivation was based on the force balance at the liquid-vapor interface, i.e., a direct application of the Young-Laplace equation.[18]

For the case of a sessile drop, the reader is referred to the work of D. N. Staicopolus[19] for a complete numerical solution of the Bashforth-Adams equation. An approximate analytical solution of a similar equation has been worked out by P. Concus[20] for calculation of the equilibrium meniscus in a vertical right circular cylinder.

In the current analysis, a direct integration of Eq. (8) subject to a given contact angle is carried out using numerical methods. Before presenting the numerical solution, however, certain points must be clarified:

1. The liquid-vapor interfacial tension is assumed to be constant throughout the calculations regardless of the position and curvature of the interface. This assumption is justified because the radii of curvature of interest in the present case are in the range of 0.01 cm, which is several magnitudes larger than the case studied by Tolman,[21] Kirkwood and Buff,[22] and Benson and Shuttleworth.[23] These authors have found that the surface tension of a small droplet decreases with increasing curvature. Tolman estimated that a 4 per cent drop in the surface tension would occur if the diameter of a droplet was in the order of 10^{-6} cm;

2. The liquid is assumed to be incompressible, and the effect of the vapor pressure on the liquid-vapor surface tension is neglected;

3. The contact line is assumed to be ideal. An ideal contact line means that two mathematically defined surfaces meet together. Thus, the line should be infinitesimal and no liquid film exists beyond the line. In conjunction with this, we note that the validity of Young's equation for the contact angle has long been claimed by Gauss[24] and Gibbs[14] and more recently by Johnson,[25] and Goodrich.[26] For arguments advocating its invalidity, however, the reader is referred to a recent paper by G. J. Jameson and M. C. G. del Cerro.[27]

Numerical solutions of the Bashforth-Adams equation (Equation (8)) satisfying the end-point conditions Equation (9) have been obtained. Figure 3 shows a set of typical solutions obtained for the liquid deuterium enclosed in a GMB for different values of contact angle. The GMB target chosen was 67 μm in inner radius, of 3 μm thickness, and was assumed to be at a uniform temperature of 24 K. For ease of comparison with the experimental results, which is to be made in the future, the room-temperature D_2-fill pressure of the target was chosen to be 110 atm. This fill pressure, along with the dimensions and temperature of the target, allows one to determine the amount of liquid deuterium inside the target using the equation of state.[28]

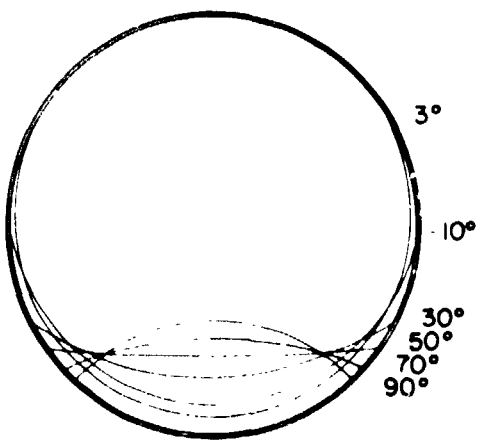

Figure 3. Numerical solutions of the Bashforth-Adams equation for various contact angles. The inner radius of the GMB is 67 μm, the wall thickness is 3 μm, and the temperature is 24 K. The liquid enclosed is deuterium and the fill pressure is 110 atm at room temperature.

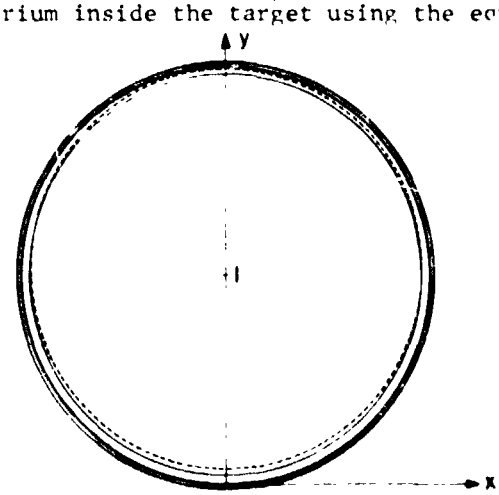

Figure 6. Numerical solutions of the Augmented Bashforth-Adams equation. The solid line is for $B_{SL} = 4.277 \times 10^{-56}$ erg-cm^6 and the broken line is for $B_{SL} = 4.277 \times 10^{-58}$ erg-cm^6. The volume of liquid deuterium is 1.208×10^{-7} cm^3 and the temperature is 28 K. The inner radius of the SMS is 67 μm and the wall thickness is 3 μm.

As clearly seen from Figure 3, the location of the contact line between liquid, solid, and gas rises as the value of the input contact angle (one of the end-point conditions, Equation (9)) is decreased. This is simply because of the fact that the smaller the contact angle, the larger is the area wet by the liquid. For zero contact angle, it is, therefore, believed that the liquid will wet the entire target substrate, resulting in a continuous liquid layer. In this case, there will be a gas bubble inside the target completely surrounded by the liquid--a situation not possible in the case of a sessile drop sitting on a flat surface.

Although different input values of the contact angle were used at the same temperature to produce the results in Figure 3, in reality, there can only be one correct contact angle corresponding to a given temperature. Since this correct contact angle is not theoretically available as a function of temperature for the current problem, it must be measured experimentally. Good and Ferry measured the contact angle between liquid hydrogen and a few different materials and reported that it was zero for all the materials studied.[29] Neither the details of the experimental arrangement nor the ranges of the observation temperatures were, however, included in their report. Considering the difficulties involved in maintaining a stable cryogenic environment and, in particular, the difficulties in creating and verifying an isothermal environment, it might perhaps not be totally unreasonable to suggest that the work of Good and Ferry be re-examined, or even redone using carefully designed, more modern equipment for all liquid hydrogen temperatures.

Assuming now that the contact angles of liquid hydrogen and, according to that of liquid deuterium are zero, it is most probable that the liquid deuterium contained in an SMS exists in the form of a continuous layer.[12,13] It is for this reason that we now go back to the Bashforth-Adams equation and see if it can adequately give rise to a continuous liquid layer solution.

Profile of a continuous liquid layer inside a spherical microshell

Let us now consider a situation where the liquid inside an SMS forms a continuous layer, i.e., no liquid-vapor-solid contact line. The coordinate system used in this case is shown in Figure 4a. Following the same procedures previously used, and considering only the terms pertaining to the gravitational force and the liquid-vapor interfacial tension, one can easily derive a differential equation, which is identical to Eq. (8). The boundary conditions are, however, different. Since the gravitational force is chosen acting parallel to the y axis, the profile of the vapor void (or the bubble) should also be symmetric about the y axis. Therefore, the boundary conditions for the bubble are

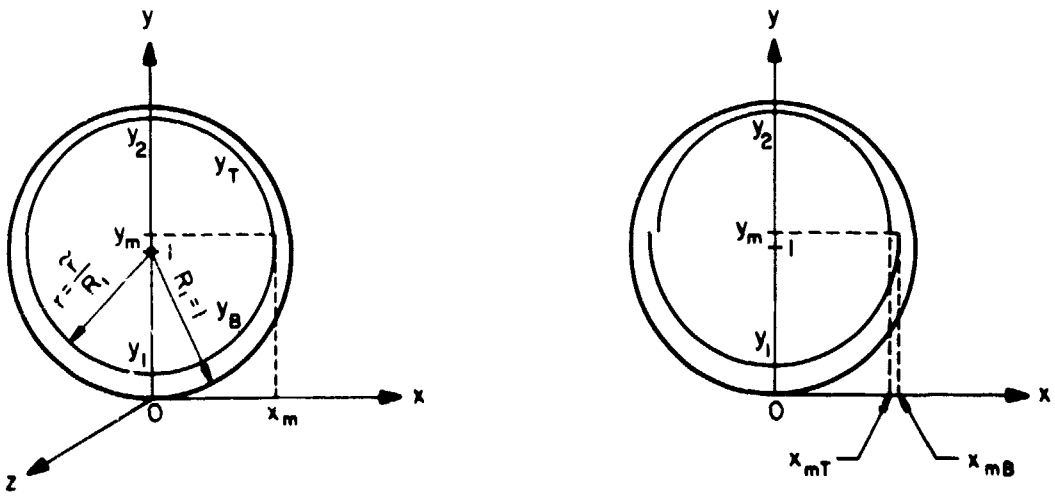

Figure 4. (a) Coordinate systems used in the continuous liquid layer case. At $x = x_m$ and $y = y_m$, x' is equal to zero. (b) Numerical solution of Bashforth-Adams equation with one boundary condition satisfied, i.e., at $x = 0$: $x' = \infty$. Note that $x_{mB} > x_{mT}$ at $x' = 0$.

$$\begin{aligned} &(1)\quad x' = \infty \quad \text{at } x = 0, \quad y = y_1 \\ &(2)\quad x' = \infty \quad \text{at } x = 0, \quad y = y_2 \end{aligned} \tag{11}$$

Before finding the numerical solutions of Equations (8) and (11), it is worthwhile to study Equation (8) somewhat more carefully. Upon integration, Equation (8) gives rise to

$$x' = \frac{\pm\left[x^2 - \int_0^x \bar{x}(\alpha + \beta y_{B,T})\, d\bar{x}\right]^2}{\int_0^x \bar{x}(\alpha + \beta y_{B,T})\, d\bar{x}} \tag{12}$$

where $y_{B,T}$ denotes the two values of y corresponding to a single value of x: in the region where x' is positive, y_B is used, with B denoting the "Bottom"; and in the region where x' is negative, y_T is used, with T representing the "Top". From Equation (12) one finds that where x' = 0, that is, when x takes on the maximum value, X_m, the values of x are given by

$$x_{mB} = \int_0^{x_{mB}} \bar{x}(\alpha + \beta y_B)\, d\bar{x} \quad , \text{ and} \tag{13a}$$

$$x_{mT} = \int_0^{x_{mT}} \bar{x}(\alpha + \beta y_T)\, d\bar{x} \quad , \tag{13b}$$

where the subscripts "B" and "T" again refer to "Bottom" and "Top," respectively. Because α and β are constants and $y_B \neq y_T$, Equation (13) implies that one has two different values of x at x' = 0. Referring to Figure 4b, since y_T is always larger than y_B, one deduces that

$$x_{mB} > x_{mT} \tag{14}$$

This deduction is clearly physically contradictory because no bubble can exist if there is a discontinuity in the liquid-vapor interface. Consequently, there will be no solution to Equation (8) which can satisfy the bubble boundary conditions Equation (11).

The numerical solutions of Equation (8) indeed illustrate this point.[30] Only one of the two boundary conditions Equation (11) is satisfied, i.e., either $x'_B = \infty$ at x = 0, but $x'_T = \infty$ at $x \neq 0$; or $x'_T = \infty$ at x = 0, but $x'_B \neq \infty$ at x = 0. It is obvious that some forces acting on the bubble that are different from the gravitational force and liquid-vapor interfacial tension are left out of the theory hitherto considered.

There are several types of forces among molecules and atoms[31]: the attactive forces are primary (chemical) bonds, metallic bonds, and secondary (physical) bonds, whereas the repulsive forces are Born repulsions. Primary bonds and metallic bonds are usually strong, and are the basic forces responsible, for example, for forming different stable substances on earth. Secondary bonds are the long-range but weak attraction forces among atoms and molecules and are generally called van der Waals forces.

In fact, van der Waals forces are a collective term for the four different forces, namely, the Debye induction force between a permanent dipole and a neutral molecule,[32] the Keesom orientational force between two freely rotating permanent dipoles,[33] the London-dispersion force due to electron fluctuations around nuclei,[34] and the Margenau force arising from the dipole-quadrupole interaction.[35] Since the liquid of our interest is deuterium or deuterium-tritium mixture and they are nonpolar neutral molecules, only the London-dispersion force is considered. The Born repulsion force is also neglected because it is inverse twelfth power of distance and thus quickly dies out as the distance is increased. The typical effective distance of the Born repulsion force is about 7 A.

Two approaches are widely used to calculate the total attraction energy of the London-van der Waals type between two macroscopic bodies. One is London-Hamaker's approach[34,36] in which the additivity of the London-van der Waals forces is assumed. The other is Lifshitz's macroscopic approach[37] in which the attraction energy is directly calculated from the imaginary parts of the complex dielectric constants of the media, especially their far ultraviolet portions.[38] Lifshitz's approach is thought to be better than that of London and Hamaker, especially in the case where the separation distance between two macroscopic bodies is large. This is mainly due to the additivity assumption and the intrinsic characteristics of the dispersion forces.

The London-van der Waals forces are electromagnetic-like forces, so they will be subject to retardation, i.e., at large separations the forces will be reduced because the finite time required for their propagation causes a phase difference between the electronic oscillations of the interacting molecules. Because of this retardation effect, the attraction energy calculated by London-Hamaker's approach will be over-estimated for molecules with large separations.[39] When the retardation effect is put into the calculation, as Casimir

and Polder,[40] and Overbeck[41] did, the two approaches usually have differences within an acceptable range.[39,42,43]

To avoid the mathematical difficulties and the scarcity of the data required of the Lifshitz's macroscopic approach, the London-Hamaker's approach is adopted. The nonretarded London-van der Waals forces are considered first. The effects of retardation then follow.

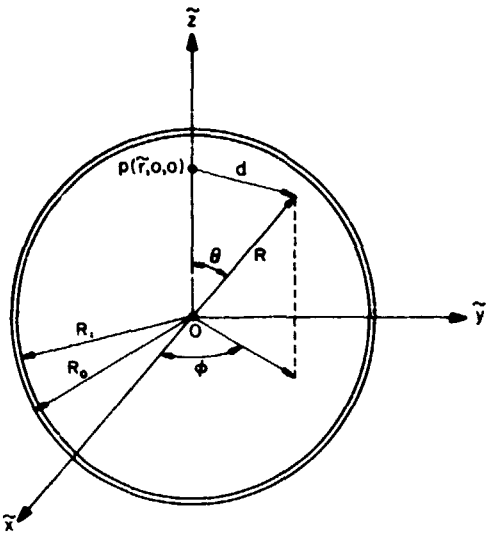

Figure 5. Spherical coordinate system used in the calculation of the London-van der Waals attraction energy between the liquid molecule at $p(\tilde{r},o,o)$ and the spherical substrate with inner radius equal to R_i and outer radius equal to R_o.

The coordinate system used is shown in Figure 5. The energy due to the London-van der Waals forces of a liquid molecule at the point $p(\tilde{r},o,o)$ is then expressed as

$$E_p(\tilde{r}) = N_s \int_{V_s} dv\, U(d) \tag{15}$$

where the London potential $U(d) = -B_{SL}/d^6$ with B_{SL} denoting the London constant between the solid (substrate) and liquid molecules; d is the distance between the substrate and liquid molecules; N_s is the number density of the substrate molecules; and V_s is the volume occupied by the substrate. Noting the azimuthal symmetry of the system, application of the cosine rules enables one to rewrite Equation (15) as

$$E_p(\tilde{r}) = -2\pi B_{SL} N_s \int_{R_i}^{R_o} R^2 dR \int_{-1}^{+1} d\mu \frac{1}{[R^2 + \tilde{r}^2 - 2\tilde{r}R\mu]^3} \tag{16}$$

where $\mu = \cos\theta$.

After straightforward integration, Equation (16) becomes

$$E_p(\tilde{r}) = \frac{+4\pi}{3} B_{SL} N_s \left[\frac{R_o^3}{[R_o^2 - \tilde{r}^2]^3} - \frac{R_i^3}{[R_i^2 - \tilde{r}^2]^3}\right] \tag{17}$$

The total energy due to the London-van der Waals forces between the liquid and the solid wall is then

$$E_{LVDW} = N_L \int_{V_L} dv\, E_p(\tilde{r}) \tag{18}$$

where N_L is the number density of the liquid and V_L is the volume occupied by the liquid.

In terms of the normalized cylindrical coordinate system defined in Figure 4a, Equation (18) is

$$E_{LVDW} = 2\pi N_L \int_{y_1}^{y_2} dy \int_o^x x\, dx\, E_p(r) \tag{19}$$

where

$$E_p(r) = \frac{4}{3R_i^3} \pi B_{SL} N_s \left[\frac{R_e^3}{[R_e^2 - r^2]^3} - \frac{1}{(1 - r^2)^3}\right]$$

$$r = \sqrt{x^2 + (y - 1)^2}$$

$$R_e = \frac{R_o}{R_i}$$

Following the same mathematical procedures previously used (i.e., the calculus of variations), one obtains

$$\frac{x''}{[1 + (x')^2]^{3/2}} - \frac{1}{x[1 + (x')^2]^{1/2}} = -[\alpha + \beta y + \bar{A}\, D(x,y)] \tag{20}$$

where

$$\bar{A} = \frac{4 - B_{SL} N_s N_L}{3 \gamma_{LV} R_i^2}$$

$$D(x,y) = \frac{R_e^3}{(R_e^2 - r^2)^3} - \frac{1}{(1 - r^2)^3}$$

and the rest of the symbols are as defined in Equation (7). This equation is similar to the Bashforth-Adams equation Equation (8), except that an extra term resulting from the London-van der Waals energy is added. For this reason, we name Equation (20) as the "Augmented Bashforth-Adams equation."

Integrating Equation (20) once and applying the bubble boundary conditions Equation (11), one has

$$\beta V_v + 2\pi\bar{A} \int_o^{x_m} x[D_T(x,y_T) - D_B(x,y_B)]\, dx = 0 \tag{21}$$

where V_v is the specific volume of the vapor void, or the bubble (i.e., the actual volume of the void divided by R_i^3), the subscript T denotes the upper (top) portion of the bubble where $x' > 0$; and the subscript B denotes the lower (bottom) portion of the bubble where $x' < 0$. From Equation (21), one can easily see that as β approaches zero and/or $\bar{A}$ approaches infinity, $[D_T(x,y_T) - D_B(x,y_B)]$ will take on a value which is vanishingly small. Or, putting it in another way, at either or both of these two limits, the thickness of the liquid layer is uniform, or the bubble is a complete sphere. In practice, however, the values of $\bar{A}$ and β are finite and, therefore, the thickness of the liquid layer at the bottom of an SMS is always larger than that at the top.

The numerical solutions of Equation (20) satisfying the bubble boundary conditions Equation (11) are plotted in Figure 6. Note that there is only one unique solution for each set of parameters used. The SMS chosen is 67 μm in inner radius, 3 μm in thickness, and contains liquid D_2 of volume 1.208×10^{-7} cm^3. The calculations are done for two different values of the London constant B_{SL}. As expected, larger B_{SL} produces a liquid layer more uniform in thickness. This effect is more clearly demonstrated by Figure 7 in which both the top and bottom thicknesses of the liquid layer are plotted as a function of B_{SL} for two different values of liquid D_2 volume. That a larger B_{SL} is required to support a thicker uniform layer is clearly shown in the figure, which is consistent with the competing nature of the gravity and the van der Waals attraction.

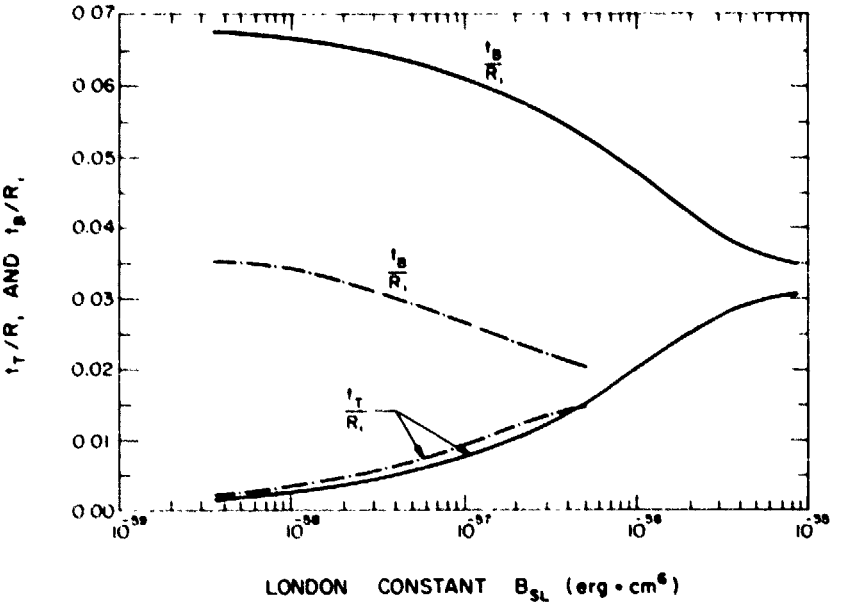

Figure 7. Equlibrium top and bottom thicknesses of liquid deuterium layer inside an SMS at 28 K. The target has inner radius of 67 μm and wall thickness of 3 μm. The broken lines are for the liquid volume of 6.47×10^{-8} cm^3 and the solid lines are for 1.208×10^{-7} cm^3.

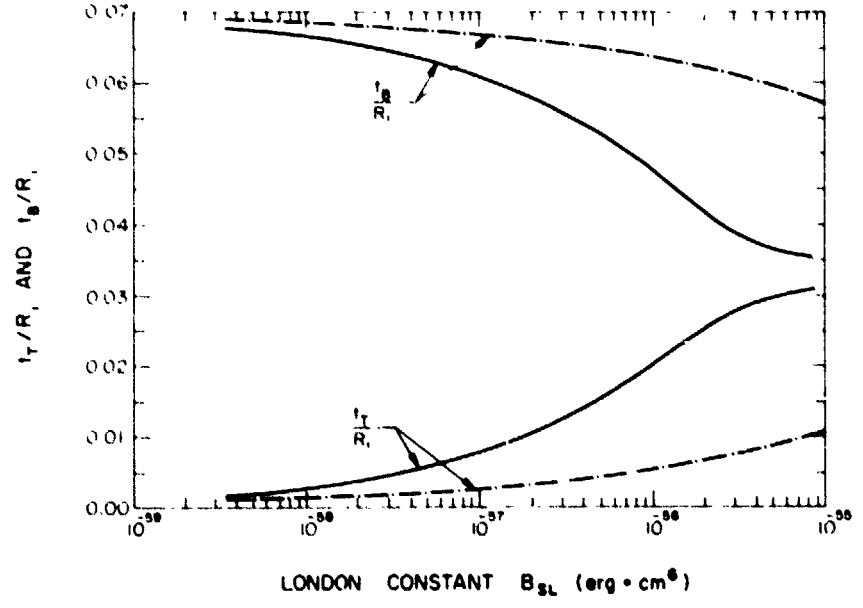

Figure 8. Comparison of equilibrium top and bottom thicknesses of liquid deuterium layer for nonretarded (solid lines) and retarded (broken lines) London-van der Waals forces. The inner radius of the SMS is 67 μm and its wall thickness is 3 μm. The volume of liquid deuterium is 1.208×10^{-7} cm^3 and the temperature is 28 K. λ_c used in the calculation of retarded London-van der Waals forces is 10^{-5} cm.

Since the wall thickness of the SMS and the thickness of the liquid layer are generally in the order of 1 μm, the retardation effect of the London-van der Waals forces could be significant as pointed out by Casimir and Polder.[40] To include such a retardation effect,[41] a correction function has been introduced into the London potential by Overbeek:

$$U(d) = -\frac{B_{SL}}{d^6} f(p) \tag{22}$$

where $p = 2\pi d/\lambda_c$ with λ_c being the characteristic wavelength of the electronic oscillation of atoms; and

$$f(p) = \begin{cases} 1.01-0.14\ p\ , & \text{for } 0 < p < 3 \\ 2.45p^{-1} - 2.04p^{-2}\ , & \text{for } 3 < p < \infty \end{cases}$$

Unfortunately, this formula is not easily applicable to our case since two separate functions are involved in two different ranges. Schenkel and Kitchener[44] have found an approximation for f(p) for the range, $1 < p < \infty$. According to these authors, the deviation in the values of f(p) is less than 5% within this range. The Schenkel-Kitchener approximation is

$$f(p) \simeq \frac{2.45}{p} - \frac{2.17}{p^2} + \frac{0.59}{p^3} \tag{23}$$

Replacing the London-potential U(d) in Equation (15) with this approximation (Equations (22) and (23)) and carrying out the straightforward, yet tedious, integration, one obtains a lengthly expression for the retarded London-van der Waals attraction energy between a liquid molecule at point p(r̂,o,o) and the entire substrate of thickness of $(R_0 - R_i)$ (see Figure 5).[30]

This expression has been used in conjunction with the Augmented Bashforth-Adams approach to determine the retardation effect of the London-van der Waals forces. Plotted in Figure 8 are the equilibrium top and bottom layer thicknesses of the liquid deuterium inside an SMS of inner radius 67 μm for various strengths of the London constant. The temperature of the SMS is 28 K and the volume of the liquid deuterium is 1.208×10^{-7} cm^3. As expected, the thickness of the top liquid layer is smaller than the case where the retardation effect is not included.

Note that the Augmented Bashforth-Adams equation Equation (20) with the retarded London-van der Waals energy term is only good within the range $1 < p < \infty$. This range might be extended down to $p = 0.5$, with a slightly larger error, as pointed out by Schenkel and Kitchener.[44] In general, λ_c is in the order of 10^{-5} cm, so that $p = 0.5$ corresponds to $d \sim 100$ Å. Consequently, as long as the top liquid layer thickness (i.e. the smaller thickness) is larger than 100 Å, the error in the solution of this equation will be negligible.

Finally, it must be pointed out that the liquid-vapor interfacial tension has been assumed to be constant throughout the calculations, which might turn out to be an important source of error.

Conclusion

An "Augmented Bashforth-Adams" equation, Equation (20), appropriate to a spherical substrate, has been derived for the first time by including the London-dispersion force as the two-body interaction force between the liquid and substrate molecules. This was prompted by a proof presented in this work that the Bashforth-Adams equation, Equation (8), has no solution subject to the boundary conditions Equation (11) required of a continuous liquid layer. The choice of the London-dispersion force was specifically motivated by the desire to describe the liquid hydrogen behavior inside a spherical microshell ICF target, and was justified by the fact that liquid hydrogen consists of nonpolar neutral molecules.

Considering the fact that most of the previous work on the thin-film phenomena, of which a wealth of literature[27,45] exists, has only dealt with either plane- or cylinder-like geometries, the principal contribution of the present work is to have formulated a theory appropriate to a spherical substrate.

It is hoped that with this work headway has been made toward an active investigation of the thin-film phenomena involving spherical geometry, not only for its own scientific merit, but also for a very interesting practical application - namely, the ICF target research.

Acknowledgment

One of us (KK) would like to thank Chun Huh of Exxon Production Research for many useful suggestions.

References

1. Work supported by USDOE under LLNL Subcontract 8320003.
2. R. J. Mason and R. L. Morse, Nuc. Fusion 15, 935 (1975).
3. R. J. Mason and R. L. Morse, Phys. Fluids 78, 814 (1975).
4. R. J. Mason, Nuc. Fusion 15, 1031 (1975).
5. T. M. Henderson, et al., Laser Interaction and Related Plasma Phenomena, ed. H. J. Schwarz and H. Hora (Plenum Publishing Corp., New York, 1977), Vol. 4A.
6. T. M. Henderson et al., Advances in Cryogenic Engineering (Plenum Press, New York. 1975), Vol. 21.
7. E. R. Grilly, Rev. Sci. Instrm. 48, 148 (1977).
8. J. R. Miller, Advances in Cryogenic Engineering, (Plenum Press, New York, 1978), Vol. 23.
9. T. M. Henderson, et al., Advances in Cryogenic Engineering (Plenum Press, New York 1978), Vol. 23.
10. K. Kim, B. J. Smoot, R. L. Woerner and C. D. Hendricks, Appl. Phys. Lett. 31, 282 (1979).
11. K. Kim and H. Rieger, Appl. Phys. Lett. 37, 425 (1980).
12. J. Fanning, L. Mok, K. Kim and T. P. Bernat, Bull. Am. Phys. Soc 25, 933 (1980).
13. T. P. Bernat and K. Kim, Proc. ICF Conf., OSA/IEEE, San Diego, CA (Feb. 1980).
14. J. W. Gibbs, Trans. Connecticut Acad. Arts Sci. 3, 343 (1877).
15. See, for example, F. B. Hildebrand, Methods of Applied Mathematics, (Prentice-Hall, Inc., New Jersey, 1965), 2nd edition, p. 139.
16. T. Young, Phil. Trans. Roy. Soc. London 95, 65 (1805).
17. F. Bashforth and J. C. Adams, An Attempt to Test the Theory of Capillary Action (Cambridge University Press and Deighton, Bell and Co., 1892).
18. P. S. de Laplace, Mechanique Celeste, Suppl. au X Livre, Coureier, Paris, 1805.
19. D. N. Staicopolus, J. Colloid Sci. 18, 793 (1963); 17, 439 (1962); 23, 453 (1967).
20. P. Concus, J. Fluid Mech. 34, 481 (1968).
21. R. C. Tolman, J. Chem. Phys. 17, 333 (1949).
22. J. G. Kirkwood and F. P. Buff, J. Chem. Phys. 17, 338 (1949).
23. G. C. Benson and R. Shuttleworth, J. Chem. Phys. 19, 130 (1951).
24. K. F. Gauss, Werke (Göttingen, 1877), Vol. 5, pp. 287-292.
25. R. E. Johnson, J. Phys. Chem. 63, 1655 (1959).
26. F. C. Goodrich, Surface and Colloid Science, ed. Matijevic (1969), Vol. 1.
27. G. J. Jameson and M. C. G. del Cerro, J. Chem. Soc. Faraday Trans. I.72, 883 (1976).
28. P. C. Souers, "Cryogenic Hydrogen Data Pertinent to Magnetic Fusion Energy," Lawrence Livermore National Laboratory, Report UCRL-52628 (1979).
29. R. J. Good and G. V. Ferry, Adv. Cryo. Eng. 8, 306 (1963).
30. L. Mok, K. Kim, and T. P. Bernat (To be published).
31. F. Z. London, Trans. Faraday Soc. 33, 8 (1937)
32. P. Debye, Phys. Z. 21, 178 (1920).
33. W. H. Keesom, Phys. Z. 22, 129 (1921).
34. F. Z. London, Phys. Z. 63, 245 (1930).
35. H. Margenau, Phys. Rev. 38, 747 (1931).
36. H. C. Hamaker, Physica 4, 1058 (1937).
37. E. M. Lifshitz, Sov. Phys. JETP 2, 73 (1956).
38. H. Krupp, "Particle Adhesion Theory and Experiment," Advances in Colloid and Interface Science (Elsevier Publishing Co., Amsterdam, 1967), p. 111.
39. J. Gregory, "The Calculation of Hamaker Constants," Advances in Colloid and Interface Science (Elsevier Publishing Co., Amsterdam, 1969), p. 396.
40. H. B. G. Casimir and D. Polder, Phys. Rev. 73, 360 (1948).
41. J. Th. G. Overbeck, Colloid Science, ed. H. R. Kruyt (Elsevier Publishing Co., London, 1952).
42. T. D. Blake, J. Chem. Soc. Faraday Trans. I, 192 (1975).
43. A. Sheludko, "Thin Liquid Films," Advances in Colloid and Interface Science (Elsevier Publishing Co., Amsterdam, 1967), p. 390.
44. J. H. Schenkel and J. A. Kitchener, Trans. Faraday Soc. 56, 161 (1960).
45. For a recent review, see, for example: K. K. Mohanty, H. T. Davis, and L. E. Scriven, Proc. 3rd Int. Conf. Surface Colloid Sci., Stockholm, Sweden, Aug. 20-25, 1979.